# CHARACTERIZATION OF STRESS CORROSION CRACKING IN AA2024-T3 BY X-RAY RADIOGRAPHY

Xiaodong Liu[1], G. S. Frankel[1], B. Zoofan[2] and S. I. Rokhlin[2]
[1]Fontana Corrosion Center, Department of Materials Science and Engineering
[2]Department of Industrial, Welding and Systems Engineering
The Ohio State University, Columbus, OH 43210, USA

ABSTRACT

A new non-destructive evaluation approach was developed to investigate stress corrosion cracking in AA2024-T3. A microfocal x-ray radiography technique was employed to image multiple intergranular stress corrosion cracks in situ. A modified ASTM G49 stressing jig was used to apply a fixed tensile displacement to a thin sheet sample and a novel electrochemical cell containing flowing 1 M NaCl was attached to the edge of the sample. Potentiostatic polarization was applied at a potential that promoted intergranular corrosion. The initiation and growth of multiple intergranular stress corrosion cracks have been characterized. The kinetics of intergranular stress corrosion cracking growth was found to be in good agreement with the results of a completely different technique, foil penetration. Interestingly, in many experiments the deepest crack at the beginning of the experiment was found to slow and stop growing, and was surpassed by another crack that eventually penetrated through the sample. The possible mechanisms underlying this competition between cracks are discussed.

## 1 INTRODUCTION

Stress corrosion cracking (SCC), which involves the combined effects of stress, an aggressive environment, and a susceptible microstructure, has been investigated extensively for decades. SCC of high strength Al alloys is almost always intergranular in nature [1-3]. In contrast, intergranular corrosion (IGC) is attack at grain boundaries that takes place in the absence of applied stress as a result of a variation in the microstructure at or near grain boundaries. In trying to sort out the effects of stress on IGC and SCC, it would be useful to be able to image the various forms of corrosion in situ. However, few in situ non-destructive evaluation (NDE) approaches exist to study IGC and SCC.

Recently, Zhao et al. used in situ x-ray radiography to study IGC and exfoliation corrosion in AA2024 and AA7178. [4]. Exfoliation corrosion is a form of IGC that occurs on surface of wrought Al alloys [5, 6]. The radiographic images presented by Zhao et al. provided information on the initiation and growth kinetics of a full population of IGC sites. Standard experimental approaches for the study of SCC kinetics, such as the double cantilever beam (DCB) specimen, are constrained to have only a single crack. However, multiple cracks can exist in real structures. The ability to image and study samples containing multiple cracks is of great interest. The interaction of stress and electrochemical reactions can alter the local environment at an IGC tip, which might assist or slow down growth rate, or favor the SCC initiation at other sites. There is a close connection between IGC and IGSCC; IGSCC can be considered to be stress-assisted IGC, particularly if the mechanism of IGSCC is anodic dissolution rather than hydrogen embrittlement.

While much is known about SCC of Al alloys, there are still many unresolved issues regarding the effects of stress on localized corrosion. The transition between IGC and IGSCC is not fully understood. For instance, if the microstructure is elongated in a direction that is not perpendicular to the applied stress, how does IGC turn into a crack? It is generally assumed that a resolved tensile stress normal to a crack tip is required for SCC propagation. How does tensile stress parallel to the crack tip or compressive stress normal to the crack affect IGC advance? The

primary mechanism for SCC in 2xxx series Al alloys is commonly regarded to be anodic dissolution [7], but this is disputed [8] because the local hydrogen evolution always accompanies the anodic dissolution in Al cracks, so effects of hydrogen embrittlement cannot be easily ruled out.

In the current study, a novel electrochemical cell associated with a modified ASTM G49 stressing jig was used along with x-ray microfocal radiography to study SCC. The sensitivity of the measurement will be evaluated using the foil penetration technique, which determines the kinetics of localized corrosion growth by measuring the penetration time at the fastest growing site [9-11].

## 2 EXPERIMENTAL

Samples were machined from a 19 mm thick wrought AA2024-T3 plate (Cu 4.5%, Mg 1.45%, Mn 0.57%, Si 0.11%, Fe 0.25%, Zn 0.09%, Ti 0.02%, Cr 0.01%, and other elements total 0.05% max) purchased from Metalmen Sales, Inc. Thin sheet samples were cut in specific orientations relative to the rolling direction with nomenclature, as shown in Figure 1a. The three perpendicular directions are denoted as the longitudinal (L, along the rolling direction), short-transverse (S, through-thickness), and transverse (T) directions. The orientation of a stressed sample is noted by two perpendicular orientations, the first indicating the nominal direction of corrosion propagation and the second indicating the direction of applied stress. For instance, an L-S sample was stressed in the S or through-thickness direction and corrosion proceeded in the L or longitudinal direction. Stress was applied using a modified ASTM G49 fixed-displacement jig described previously [11]. For samples stressed in the S or through-thickness plate direction, laser-welded tabs were used to allow gripping by the stressing jig, which is the same approach that was used in the stressed foil penetration experiments [11]. The samples were typically stressed at an initial strain of 0.18%, which is in the elastic region, less than halfway to yield according to the stress strain curve measured in a standard tension testing machine on an AA2024-T3 blank.

Pieces 80 mm long and 5 mm wide were cut from the plate using electrical discharge machining (EDM), and reduced to a thickness of 1.05 mm by grinding. The surfaces were polished to 1200 grit in methanol or ethanol to minimize corrosion. The stress was applied along the sample length direction, and a specially-designed electrochemical cell was positioned on the thin edge of the sample exposing only that edge to solution, Figure 1b. The nominal direction of corrosion was perpendicular to that edge, through the width of the sample.

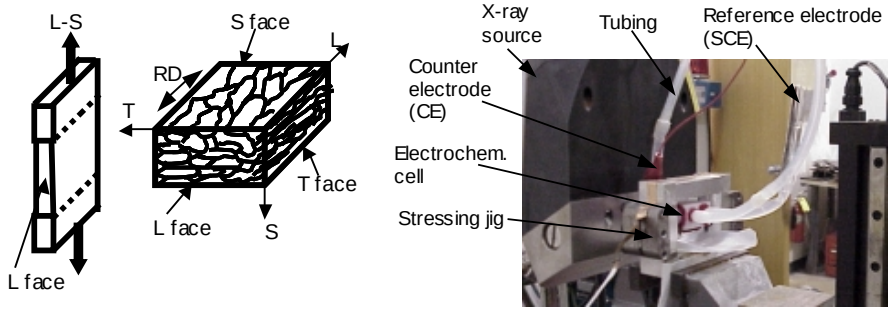


(a) (b)

Figure 1: (a) Notation and configuration of the tested sheet sample. (b) A stressed sample constrained in stressing jig with electrochemical cell, reference electrode, counter electrode and solution tubing in front of the x-ray source.

The cell was a rectangular piece of Teflon with nominal dimensions of 15 x 15 x 23 mm. Machined in one side of the cell was a 1.05 x 18.5 mm slot, and two lips that were 0.5 x 1.5 x 23 mm in dimension extended from the edges of the slot. The thin edge of the sample was slipped between the lips and exposed to the inside of the cell through the slot. Four holes were drilled and threaded into the side walls of the cell to allow connection of 1/8" I.D. nylon nozzles for attachment of tubing. The tubing was used to accommodate pumping of electrolyte and to provide access for a saturated calomel reference electrode (SCE) and a counter electrode. A strip sample was inserted in the stressing jig cell, the desired displacement was applied, and then the cell was mounted on the edge of the sample. Finally, the cell was sealed along the lips with Miccrostop lacquer. The exposed area was about 0.2 $cm^2$ (1.05 x 18.5 mm). The length of the slot allowed for testing of the sample section far from the weld and heat affected zone for samples with welded tabs. Because of the small volume of the cell chamber, the 1.0 M NaCl solution was circulated continuously by a mini pump from a reservoir through the cell and past the sample. The solution in the reservoir was refreshed every 24 h. The sample was potentiostatically polarized at –580 mV SCE to promote IGC of the AA2024-T3 and the current was recorded during the experiment.

Microfocal radiographic imaging was performed using a 225-kV, 3-mA x-ray source with 3-5 μm focal size and a positioning system with 2 μm linear resolution and 0.01° rotational resolution [12]. A schematic of the radiographic setup is shown in Figure 2. X-rays illuminated the sample width, penetrated through the sample thickness and projected an image on the x-ray intensifier unit or Eastman Kodak AA film positioned on that unit. The projection magnification was obtained by the ratio of the distance between the x-ray source and the film to the distance between the source and the sample, i.e. $d_i/d_0$, as shown in Figure 2. X-ray images were recorded periodically during the experiment. To obtain optimum resolution for a 1 mm thick Al alloy sample at 10x magnification ($d_i/d_0$=30"/3"), the source voltage and current were 40 kV and 200 μA, respectively, and the exposure time was 275 s. The processed films were digitized using a charge-coupled device (CCD) camera. X-ray microfocal radiography generates a gray-scale image in which the intensity depends on the integrated X-ray absorption through the sample thickness [12]. The absorption of X-rays varies as a result of density variations in the material. A higher density region, such as an intermetallic particle, generates a white spot on the negative X-ray film, whereas the lower density region associated with corrosion generates a dark region.

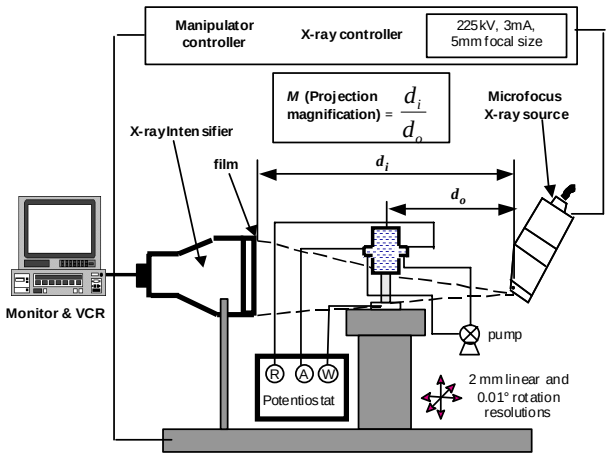


Figure 2: Schematic of the microradiographic apparatus with corrosion cell and stressed sample.

## 3 RESULTS AND DISCUSSION

Figure 3 shows radiographic images of an L-S sample with 0.18% applied strain, i.e. it was stressed in the S direction and cracks grew in the L direction. The top edge of each image was the exposed L surface of the sample. The vertical white streaks are associated with intermetallic particles aligned in the L direction in the wrought microstructure. Two horizontal white lines are also visible. The line at the sample surface is associated with a thick part of the Teflon cell and the line 1.5 mm below the surface is from the lacquer used to seal the end of the cell lips. The white scrawl patterns between the two white lines result from an excess of red lacquer along the sealing area. These patterns were used as a reference to identify the location of specific IGC sites. The intergranular cracks show up as thick, dark vertical lines. These cracks were straight and sharp and propagated along the L direction. The radiographic images are integrations of IGC and particles through the sample in the T direction, rather than reflections of continuous microstructural components in the sample. The average grain size of this particular AA2024-T3 plate at the ¼ T section is approximately 50 μm, 300 μm, and 2000 μm in the S, T, and L directions, respectively [13]. The thickness of the sample used in this study is 1.05 mm along the T direction, which indicates that the sample had 3-4 grains through the thickness. The feature labeled site 1 in Figure 3a was the first crack to form, and the crack at site 2 was found later. During the first hour of the experiment, the crack at site 1 was the longest and the fastest growing crack. However, this initial crack stopped growing, while IGC at site 2 initiated, grew faster, and ultimately overtook the first crack to become the deepest crack in the sample, as is evident in Figure 3b. This phenomenon was not an exception; almost every sample studied, in a variety of propagation and stressing orientations, exhibited a deceleration in growth of the initial crack and ultimate failure at another site. This observation is counter to the expectations of mechanical fracture in inert environments, in which the driving force of crack growth is stress intensity.

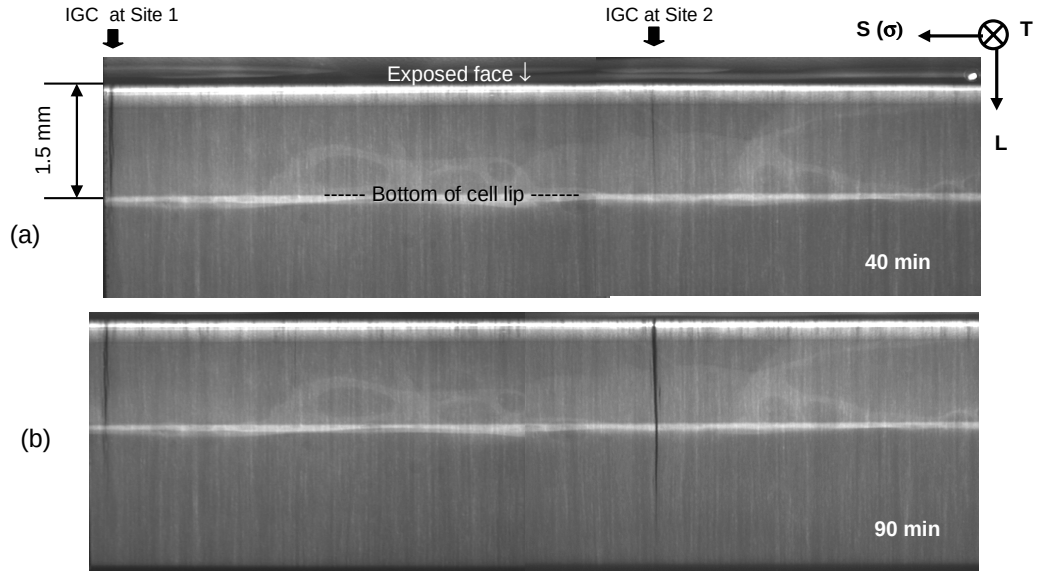


Figure 3: X-ray microfocal radiography images of IGSCC growth in L orientation in AA 2024-T3 with 0.18% strain applied in the S direction at 20x projection magnification. The potential was –580 mV SCE and the solution was 1.0 M NaCl. (a) after 40 min. (b) after 90 min.

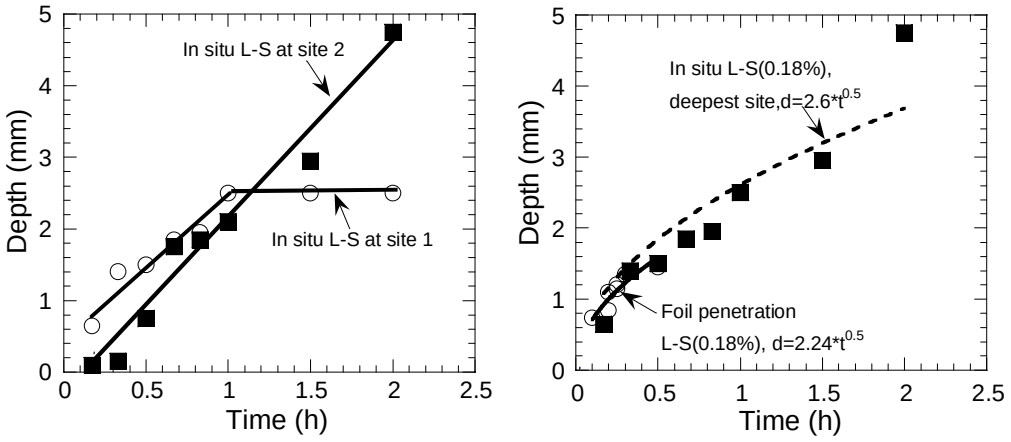


(a) (b)

Figure 4: (a) Growth rate of individual IGSCC sites in AA2024-T3 L-S sample from *in situ* radiographic images compared to foil penetration data. Site 2 (filled squares) started later but grew to failure. (b) Combination of the data from sites 1 and 2 to show the deepest site at any time (filled squares) compared to foil penetration data (open circles) [14].

The growth rate data for the two sites in the *in situ* radiographic experiment are summarized in Figure 4a. Site 1 is seen to initiate earlier than site 2 and grow to a longer length over the first hour of the experiment. However, for some reason that site stopped growing. This stifling of SCC growth is quite interesting and unexpected because of the higher stress concentration at the end of the longest site at any given time. The mechanism behind this crack stifling is not understood. However, the length of the initial crack is approximately equal to the average grain dimension in the longitudinal direction, so crack stifling might be associated with grain triple points.

Figure 4b compares the radiographic data to results from foil penetration experiments [11, 14]. The foil penetration method assesses IGC or SCC crack kinetics in a very different fashion: one side of a foil sample is exposed to solution and the time for penetration of the foil by localized corrosion is detected [15, 16]. Therefore, the foil penetration method only provides information on the deepest growing site, whereas the radiographic approach provides information on all of the sites. Figure 4b shows the depth of the deepest growth site at any given time in the radiographic experiment, which is a combination of the data from sites 1 and 2. These data almost overlie the data from the foil penetration experiments, which reflects the high sensitivity of the approach. The foil penetration technique does not provide information on the propagation rates of individual sites, only the nominal fastest rate for an ensemble of sites.

The crack stifling phenomenon observed by radiography suggests that stress-assisted dissolution at the site of highest stress concentration is not the sole driving force for SCC crack growth. It is possible that grain boundary intermetallic particles or hydrogen generated at active crack tips play a role. Alternatively, the slight redirection of grain boundaries at triple points or the exact misorientation of grains across different grain boundaries could be critical. Further investigation is required to determine the essential nature of this phenomenon.

## 4 CONCLUSIONS

1. Microfocal x-ray radiography provided images of the full population of corrosion sites in AA2024-T3and allowed for direct measurement of the kinetics of IGSCC growth of individual sites.
2. The fastest-growing crack at the beginning of the test was surpassed by another crack that ultimately penetrated the sample. The mechanism behind this crack competision is not clear as yet.

## 5 ACKNOWLEDGEMENTS

This work was supported by the United States Air Force Office of Scientific Research through Grant No. F49620-02-1-0148. The contract monitor is Lt. Col. Paul Trulove.

## 6 REFERENCES

1. M.O. Speidel, "Stress Corrosion Cracking of Aluminum Alloys", *Met. Trans. A*, **6A**(4): p.631-651 (1975).
2. H. Vogt and M.O. Speidel, "Stress Corrosion Cracking of Two Aluminum Alloys: a comparison between experimental observations and Data based on Modeling", *Corr. Sci.*, **40**(2/3): p. 251-270 (1998.).
3. R.C. Newman and R.P.M. Procter, "Silver Jbilee Review, Stress Corrosion Cracking: 1965-1990", *Brit. Corr. J.*, **25**(4): p. 259-269 (1990).
4. X. Zhao, G.S. Frankel, B. Zoofan and S.I. Rokhlin "In situ X-ray Radiographic Study of Intergranular Corrosion in Aluminum Alloys". *Corrosion*, **59**(11): p. 1012-1018 (2003).
5. ASTM STPG34, "*Test for Exfoliation Corrosion Susceptibility in 7xxx Series Copper-Containing Aluminum Alloys, EXCO Test*, ed. P.A. West, Conshohochken. PA, 1979.
6. M.J. Robinson and N.C. Jackson, "Exfoliation corrosion of high strength Al-Cu-Mg alloys: effect of grain structure", *Brit. Corr. J.*, **34**(1): p. 45-49 (1999).
7. T.D. Burleigh, "The Postulated Mechanisms for Stress Corrosion Cracking of Aluminum Alloys: A Review of the Literature 1980-1989", *Corrosion*, **47**(2): p. 89-98 (1991).
8. F. Zeides and I. Roman, "Study of Hydrogen Embrittlement in Aluminum Alloy 2024 in the Longitudinal Direction", *Mat. Sci. Eng.*, **A125**: p. 21-31 (1990).
9. F. Hunkeler and H. Bohni, "Mechanism of Pit Growth on Aluminum Under Open Circuit Conditions", *Corrosion*, **40**(10): p. 534-540 (1984).
10. W. Zhang and G.S. Frankel, "Anisotropy of Localized Corrosion in AA2024-T3", *Electrochem. Sol State. Lett.*, **3**(6): p. 268 (2000).
11. Xiaodong Liu, G.S. Frankel, B. Zoofan and S.I. Rokhlin, "Effect of Applied Tensile Stress on Intergranular Corrosion of AA2024-T3", *Corr. Sci.*, **46**: p. 405-425 (2004).
12. B. Zoofan and S.I. Rokhlin, "Microradiographic Detection of Corrosion Pitting", *Mat. Eval*, **52**(2): p. 191-194 (1998).
13. W. Zhang, Shiling Ruan, D.A. Wolfe and G.S. Frankel "Statistical Model for intergranular corrosion growth kinetics", *Corr. Sci.*, **45**: p. 353-370 (2003).
14. Xiaodong Liu, Z. Zhao, G.S. Frankel, B. Zoofan and S.I. Rokhlin, "Effects of Stress on Localized Corrosion in Al and Al Alloys," Proceedings of Triservice Corrosion Conference, Las Vegas, 2003.
15. A. Rota and H. Bohni, "Contribution to the growth kinetics of the intergranular corrosion of age-hardened Al-Cu alloys-Part1: Results of the foil penetration technique", *Werkstoffe und Korrosion*, **40**: p. 219-228 (1989).
16. A.Rota and H.Bohni, "Contribution to the growth kinetics of the intergranular corrosion of age-hardened Al-Cu alloys-Part2: Infulence of mechanical stress". *Werkstoffe und Korrosion*, **40**: p. 295-303 (1989).